Discussion of the conditional-probability function for electric fields in a plasma

Earl W. Smith
National Bureau of Standards, Boulder, Colorado 80303

Roland Stamm
Université de Provence, F-13397 Marseille 13, France

J. Cooper
University of Colorado, Boulder, Colorado 80302

(Received 12 September 1983)

The conditional-probability function plays a central role in the development of stochastic models for spectral line shapes in plasmas. We discuss some of the physical properties of this function using various analytic models as well as the results of a computer simulation.

I. INTRODUCTION

In the field of Stark broadening the class of theories known as the model microfield method (MMM) is currently of considerable interest to both theoreticians and experimentalists. This is due in part to the fact that the MMM has provided consistently better agreement with experimental data than the conventional unified or impact theories for cases where ion dynamic effects are known to be important. Nonetheless, the MMM, as currently employed,[1,2] does not produce complete agreement with experimental data. The MMM is especially intriguing because it differs radically from conventional theories, being more abstractly mathematical. At the present time, the reasons for the improved agreement with the experiment are not clearly understood nor is it clear what should be done to reduce the remaining discrepancies. A step in that direction was taken in Ref. 3 which attempts to provide a physical understanding of the MMM. In Sec. 5 of Ref. 3, it was argued that one problem with the MMM may be found in the approximation used for the electric field conditional probability function. In the present paper we will study the physical properties of this function using the computer simulation technique presented in Ref. 4 and compare these results with various analytic approximations.

Consider the electric field at some specific point in the plasma, henceforth called the test point. The conditional probability function $P(\vec{\epsilon},t \mid \vec{\epsilon}_0,0)$ gives the probability that, at the time t, this electric field will take the value $\vec{\epsilon}$, when it is known that the field was $\vec{\epsilon}_0$ at the time $t=0$. This conditional probability function must satisfy the conditions

$$\int d\vec{\epsilon} P(\vec{\epsilon},t \mid \vec{\epsilon}_0,0)=1 , \tag{1.1}$$

$$P(\vec{\epsilon},t \mid \vec{\epsilon}_0,0)\rightarrow\delta(\vec{\epsilon}-\vec{\epsilon}_0) \text{ as } t\rightarrow 0 \tag{1.2}$$

$$P(\vec{\epsilon},t \mid \vec{\epsilon}_0,0)\rightarrow P_{\rm eq}(\epsilon) \text{ as } t\rightarrow\infty \tag{1.3}$$

where $P_{\rm eq}$ is the steady-state or equilibrium distribution; $P_{\rm eq}$ is related to the well-known electric microfield distribution function[5] $P(\epsilon)$ by $P_{\rm eq}(\epsilon)=4\pi\epsilon^2 P(\epsilon)$. For the purpose of theoretical modeling, it will often be convenient to consider the joint probability distribution function Φ, which is related to P by

$$\Phi(\vec{\epsilon},t \mid \vec{\epsilon}_0,0)=P(\vec{\epsilon},t \mid \vec{\epsilon}_0,0)P_{\rm eq}(\epsilon_0) . \tag{1.4}$$

Throughout this paper, we will consider the plasma to be represented by a gas of N Debye shielded ions which do not interact with one another. The electric field for such a system may be expressed as

$$\sum_j \vec{\epsilon}_s(\vec{r}_j)=\sum_j (e\vec{r}_j/r_j^3)(1+r_j/\lambda_D)\exp(-r_j/\lambda_D) , \tag{1.5}$$

where $\lambda_D=\sqrt{kT/4\pi ne^2}$ is the Debye shielding length for a temperature T and an ion density n, and $\vec{r}_j$ denotes the position of the jth ion. For a gas of noninteracting ions, the ion trajectories will be linear so one may write $\vec{r}_j(t)=\vec{x}_j+\vec{v}_j t$, where $\vec{x}_j$ denotes the ion position at time $t=0$ and $\vec{v}_j$ is its velocity. In fact, for this model, it is possible to write a simple theoretical expression for Φ

$$\Phi(\vec{\epsilon},t \mid \vec{\epsilon}_0,0)=V^{-N}\int d\vec{x}_1\cdots d\vec{x}_N \int d\vec{v}_1\cdots d\vec{v}_N W(v_1)\cdots W(v_N)\delta\left[\vec{\epsilon}_0-\sum_j \vec{\epsilon}_s(x_j)\right]\delta\left[\vec{\epsilon}-\sum_j \vec{\epsilon}_s(r_j)\right] , \tag{1.6}$$

where $W(v)$ is a Maxwellian velocity distribution and $V=\int d\vec{x}_j$ is the volume of the system. This expression will be developed further in the Appendix. For the moment we simply note that the computer simulation which we have employed is equivalent to a numerical evaluation of Eq. (1.6).

It must be emphasized that our model of Debye shielded noninteracting ions has some clear limitations. These

limitations include the lack of dynamic shielding effects[6,7] which are known to be important for nonthermal plasmas[8] but are negligible for an equilibrium plasma. Our model also lacks three-body and higher-order ion correlations (two-body correlations are of course represented by the Debye shielding[9]) which again should be negligible for an equilibrium plasma in the classical domain where the number of ions in the Debye sphere exceeds one. Our model is of course restricted to the "low-frequency" or "ion component" of the electric microfield, consequently the high-frequency electron contribution must be added for many practical applications.

II. ANALYTIC MODELS

A. Strong diffusion models

In the MMM model originally proposed by Brissaud and Frisch,[10] $P(\vec{\epsilon},t \mid \vec{\epsilon}_0,0)$ was determined from a Markovian stochastic process which they called a "kangaroo" process. According to that model, P is the solution of the differential Chapman-Kolmogorov equation

$$\partial_t P(\vec{\epsilon},t \mid \vec{\epsilon}_0,0) = -\nu(\epsilon)P(\vec{\epsilon},t \mid \vec{\epsilon}_0,0) + \int d^3\epsilon' W(\epsilon \mid \epsilon')P(\vec{\epsilon}',t \mid \vec{\epsilon}_0,0) , \quad (2.1)$$

where $\nu(\epsilon)$ and $W(\epsilon \mid \epsilon')$ are isotropic functions (i.e., functions of $\epsilon=\vec{\epsilon}$ and $\epsilon'=\vec{\epsilon}'$) given by

$$\nu(\epsilon) = \int d^3\epsilon' W(\epsilon' \mid \epsilon) , \quad (2.2)$$

$$W(\epsilon' \mid \epsilon) = \nu(\epsilon)Q(\epsilon') , \quad (2.3)$$

$$Q(\epsilon') = \nu(\epsilon')P_{eq}(\epsilon')/\langle\nu\rangle , \quad (2.4)$$

$$\langle\nu\rangle = \int d^3\epsilon\, \nu(\epsilon)P_{eq}(\epsilon) , \quad (2.5)$$

with $P_{eq}(\epsilon)$ being the steady-state solution to Eq. (2.1), as required by the boundary condition stated in Eq. (1.3). Using Eqs. (2.2)—(2.5) and the boundary conditions of Eqs. (1.1) and (1.2), it is possible to obtain an iterative solution to Eq. (2.1) in the form

$$P(\vec{\epsilon},t \mid \vec{\epsilon}_0,0) = e^{-\nu(\epsilon)t}\delta(\vec{\epsilon}-\vec{\epsilon}_0) + \int_0^t dt_0 e^{-\nu(\epsilon)(t-t_0)}W(\epsilon \mid \epsilon_0)e^{-\nu(\epsilon_0)t_0} + \sum_{n=1}^{\infty}\int_0^t dt_n \cdots \int_0^{t_1} dt_0 \int d^3\epsilon_n \cdots \int d^3\epsilon_1 e^{-\nu(\epsilon)(t-t_n)}W(\epsilon \mid \epsilon_n)e^{-\nu(\epsilon_n)(t_n-t_{n-1})} \times W(\epsilon_n \mid \epsilon_{n-1}) \cdots e^{-\nu(\epsilon_1)(t_1-t_0)}W(\epsilon_1 \mid \epsilon_0)e^{-\nu(\epsilon_0)t_0} . \quad (2.6)$$

For our purposes, it is convenient to rewrite this function in the form

$$P(\vec{\epsilon},t \mid \vec{\epsilon},0) = \delta(\vec{\epsilon}-\vec{\epsilon}_0)f(\epsilon_0,t) + g(\epsilon,\epsilon_0,t) , \quad (2.7)$$

where $g(\epsilon,\epsilon_0,t)$ is an isotropic function of $\epsilon=|\vec{\epsilon}|$ which depends parametrically on ϵ_0 and t and $f(\epsilon_0,t) = \exp[-\nu(\epsilon_0)t]$ for the MMM process.

A more general non-Markovian model has been proposed by Seidel[11] in which he employs a class of stochastic process known as a renewal process.[12] Seidel's model, which he calls a "theta process," is derived in detail in pp. 84—93 of Ref. 13. For our purposes, we will simply note that $P(\epsilon,t \mid \vec{\epsilon}_0,0)$ for the theta process is also given by Eq. (2.7) with slightly different functions f and g.

The important point here is that P is given by the sum of a delta function at $\vec{\epsilon}=\vec{\epsilon}_0$ and an isotropic function of ϵ centered at $\epsilon=0$. The "amplitude" of the delta function decays exponentially with time while the isotropic part increases from $g=0$ at $t=0$ and approaches $P_{eq}(\epsilon)$ as $t\to\infty$. This behavior is illustrated qualitatively in Fig. 1 where the delta function is represented by a solid bar at $\vec{\epsilon}=\vec{\epsilon}_0$. The z axis points in the direction $\vec{\epsilon}_0$ and, since P is cylindrically symmetric about the z axis, we have plotted P as a function of ϵ_x and ϵ_z. This figure shows that the distribution function P is a sum of two distributions, one being the delta function at $\vec{\epsilon}=\vec{\epsilon}_0$ which decays away with time, and the other is a symmetric distribution about $\vec{\epsilon}=0$ which increases with time and finally approaches the equilibrium function $P_{eq}(\epsilon)$ as $t\to\infty$. This behavior is characteristic of a strong diffusion process in which any change in the electric field completely destroys all memory of the initial field.

B. Weak diffusion models

In Ref. 3 it was argued that a strong diffusion process would not give a good representation of the fourth-order and higher terms in a series expansion of the resolvent operator $M_c(\omega)$ used in spectral line broadening (Sec. 5 of Ref. 3). Since these are known to be important for strong collisions, it was argued that one might consider a weak diffusion model similar to a Fokker-Planck process in which the electric field would change through a series of small displacements. An example of such a model is

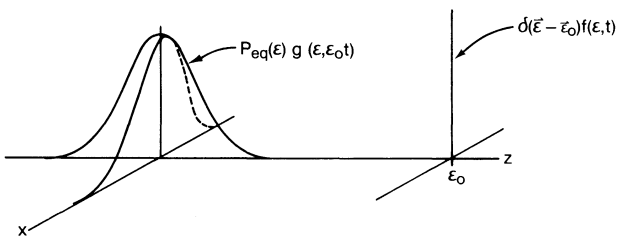

FIG. 1. Illustration of $P(\vec{\epsilon},t \mid \vec{\epsilon}_0,0)$ for the strong diffusion model. As t increases, the amplitude $f(\epsilon,t)$ of the delta function increases while the amplitude $g(\epsilon,\epsilon_0 t)$ of the equilibrium function P_{eq} decreases. The direction of the initial field $\vec{\epsilon}$ defines the z axis.

$$P(\vec{\epsilon},t \mid \epsilon_0,0)=\frac{1}{[1+\Gamma(\epsilon_0,t)]^3} \times P_{\rm eq}\left[\frac{|\vec{\epsilon}-\vec{\epsilon}_0\Gamma(\epsilon_0,t)|}{1-\Gamma(\epsilon_0,t)}\right], \tag{2.8}$$

where $\Gamma(\epsilon_0,t)$ may be any function which obeys the conditions

$$\Gamma(\epsilon_0,t)\rightarrow 1 \text{ as } t\rightarrow 0 , \tag{2.9}$$

$$\Gamma(\epsilon_0,t)\rightarrow 0 \text{ as } t\rightarrow \infty , \tag{2.10}$$

$$\int d^3\epsilon\, \epsilon^2\Gamma(\epsilon,t)P_{\rm eq}(\epsilon)=C(t) , \tag{2.11}$$

and $C(t)$ is the known[14] electric field autocorrelation function [see Eq. (3.1) of Ref. 4]. Equations (2.9) and (2.10) ensure that P will satisfy the boundary conditions specified by Eqs. (1.1)—(1.3) while Eq. (2.11) ensures that the electric field autocorrelation function will equal the known result, $C(t)$:

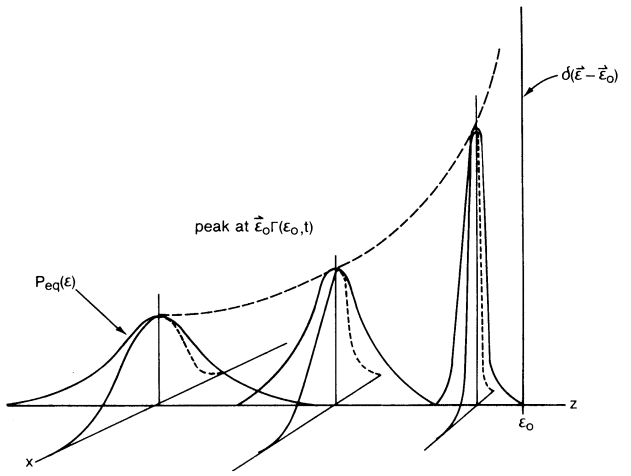

FIG. 2. Illustration of $P(\vec{\epsilon},t \mid \vec{\epsilon}_0,0)$ for the weak diffusion model showing the monotonic decrease of the peak height and the shift of the peak toward $\epsilon=0$ as t increases. The direction of the initial field $\vec{\epsilon}_0$ defines the z axis.

$$\begin{aligned}\langle \vec{\epsilon}(t)\cdot\vec{\epsilon}(0)\rangle &= \int d^3\epsilon \int d^3\epsilon_0 \vec{\epsilon}\cdot\vec{\epsilon}_0 P(\vec{\epsilon},t \mid \vec{\epsilon}_0,0)P_{\rm eq}(\epsilon)_0 \\ &= \int d^3\epsilon' \int d^3\epsilon_0[(1-\Gamma)\vec{\epsilon}'+\Gamma\vec{\epsilon}_0]\cdot\vec{\epsilon}_0 P_{\rm eq}(\epsilon')P_{\rm eq}(\epsilon_0) \\ &= \int d^3\epsilon_0\epsilon_0^2\Gamma(\epsilon_0,t)P_{\rm eq}(\epsilon_0) \\ &= C(t) .\end{aligned} \tag{2.12}$$

Since $C(t)$ is a monotonically decreasing function of t, it may be expected that Eq. (2.11) will result in a function $\Gamma(\epsilon_0,t)$ which also decreases monotonically. This being the case, the function $P(\vec{\epsilon},t \mid \vec{\epsilon}_0,0)$ given by Eq. (2.8) will be isotropically peaked about the vector $\vec{\epsilon}_0\Gamma(\epsilon_0,t)$. The width of this peak, $1-\Gamma$, will increase monotonically and, since P is normalized to unity, the peak height must decrease monotonically. This functional behavior is qualitatively plotted in Fig. 2 where again z points in the direction $\vec{\epsilon}_0$ and we have plotted P as a function of ϵ_x and ϵ_z due to cylindrical symmetry about the direction $\vec{\epsilon}_0$. In this figure we have qualitatively sketched P for four different times ranging from $t=0$ where the solid bar is used to represent the delta function at $\vec{\epsilon}=\vec{\epsilon}_0$, to $t=\infty$ where one obtains the equilibrium distribution $P_{\rm eq}(\epsilon)$ centered at $\vec{\epsilon}=0$. This is meant to show that P is an isotropic singly peaked function which broadens and shifts as time increases, gradually changing from the delta function at $t=0$ into the equilibrium distribution as $t\rightarrow\infty$. This behavior is characteristic of a weak diffusion process in which changes in the electric field are small and do not completely destroy memory of the initial field; note for example that the peak is always located on the z axis or $\vec{\epsilon}_0$ direction and the location of the peak, $\vec{\epsilon}_0\Gamma(\epsilon_0,t)$, is a function of ϵ_0.

C. Single-ion model

In this section we will consider the conditional probability function due to a single ion. This function will provide a useful approximation to $P(\vec{\epsilon},t \mid \vec{\epsilon}_0,0)$ for small t and large values of ϵ_0 which tend to be dominated by a single ion that is initially close to our test point (i.e., the point where we are evaluating the electric field). To further simplify the calculation we will use a Coulomb field rather than the shielded field in Eq. (1.1); this simplification will not produce serious errors for large ϵ. For a single ion producing a Coulomb field, Eq. (1.6) reduces to

$$\Phi_1(\vec{\epsilon},t \mid \vec{\epsilon}_0,0)=n\int d^3x \int d^3v\, W(v)\delta(\vec{\epsilon}-e\vec{r}/r^3) \times\delta(\vec{\epsilon}_0-e\vec{x}/x^3) , \tag{2.13}$$

$$W(v)=(\sqrt{\pi}v_0)^{-3}\exp(-v^2/v_0^2) , \tag{2.14}$$

where $\vec{r}=\vec{x}+\vec{v}t$, the density $n=1/V$, and $v_0=\sqrt{2kT/m}$. Using $\vec{\eta}=\vec{x}/\sqrt{e}$ and $\vec{\xi}=\vec{r}/\sqrt{e}$ we readily obtain

$$\Phi_1(\vec{\epsilon},t \mid \vec{\epsilon}_0,0)=\tfrac{1}{2}(e/\pi\epsilon^3v_0^2t^2)^{3/2}nP_{\rm eq}^H(\epsilon_0)\exp\left[-\left[\frac{\vec{\epsilon}}{\epsilon^{3/2}}-\frac{\vec{\epsilon}_0}{\epsilon_0^{3/2}}\right]^2\frac{e}{(v_0t)^2}\right] , \tag{2.15}$$

where $P_{eq}^{H}(\epsilon_0)$ is the asymptotic (i.e., large ϵ_0) Holtsmark equilibrium distribution function

$$P_{eq}^{H}(\epsilon_0)=e^{3/2}/2\epsilon_0^{9/2} . \tag{2.16}$$

Equation (2.15) could be improved slightly by using shielded fields rather than the Coulomb fields in Eq. (2.13) but the result is much more complex and provides no additional physical insight. This expression for Φ_1 does not satisfy the boundary conditions specified by Eqs. (1.1)—(1.3) when using Eq. (1.4). However, if $nP_{eq}^{H}(\epsilon_0)$ is replaced by $P_{eq}(\epsilon_0)$, Eqs. (1.1) and (1.2) are satisfied although, as $t\to\infty$, we would still have $\Phi_1\to\delta(\epsilon)$ rather than $P_{eq}(\epsilon)P_{eq}(\epsilon_0)$. The latter defect merely shows that the single-ion approximation cannot be valid in the large-t limit.

From the above discussion we conclude that the single-ion model should provide a good approximation to the functional form of the conditional probability distribution for small times t if we replace $nP_{eq}^{H}(\epsilon_0)$ by $P_{eq}(\epsilon_0)$ in Eq. (2.15). We therefore use

$$\Phi_1(\vec{\epsilon},t\mid\vec{\epsilon}_0,0)=\tfrac{1}{2}\left[\frac{1}{\pi\epsilon^3w^2t^2}\right]^{3/2}P_{eq}(\epsilon_0) \times\exp\left[-\left[\frac{\vec{\epsilon}}{\epsilon^{3/2}}-\frac{\vec{\epsilon}_0}{\epsilon_0^{3/2}}\right]^2\frac{1}{w^2t^2}\right] \tag{2.17}$$

in which w will be treated as an adjustable parameter to be determined by the computer simulation data. The adjustable parameter w will allow us to account for some of the shielding effects and, using $P_{eq}(\epsilon_0)$ rather than P_{eq}^{H}, thereby extends the utility of this function to small ϵ_0. Of course for very small t and large ϵ_0 where Eq. (2.15) is rigorously valid we expect that w should approach $v_0/\sqrt{e}$. This asymptote is shown in Fig. 13.

Equation (2.17) is similar to the weak diffusion model in that Φ_1 is peaked about some point $\vec{\epsilon}_s(\epsilon_0,t)=\hat{\epsilon}_0\epsilon_s(\epsilon_0,t)$, and this peak broadens and shifts toward smaller fields as time increases; the location of this peak can be easily determined by setting the derivative, $\partial\Phi_1/\partial\epsilon$, equal to zero. Whereas the peak for the weak diffusion model was an isotropic function of $\vec{\epsilon}$, $\hat{\epsilon}_0\Gamma(\epsilon_0,t)$, the peak in P_1 is asymmetric. In fact, by expanding Eq. (2.17) about $\vec{\epsilon}_s$ one can show that, for small values of $\delta\vec{\epsilon}=\vec{\epsilon}-\vec{\epsilon}_s$,

$$\Phi_1(\vec{\epsilon},t\mid\vec{\epsilon}_0,0)\propto\exp\left[-\frac{A-B\cos^2\theta}{w^2t^2}\left[\frac{\delta\epsilon}{\epsilon_s}\right]^2-\frac{(C+D\sin^2\theta)\cos^2\theta}{w^2t^2}\left[\frac{\delta\epsilon^3}{\epsilon_s}\right]+\cdots\right], \tag{2.18}$$

where $\cos\theta=\hat{\epsilon}\cdot\hat{\epsilon}_s$ and A,B,C,D are positive coefficients which depend on ϵ_0, ϵ_s, t, and $A>B$. This result shows that Φ_1 falls off most rapidly when $\delta\vec{\epsilon}\perp\vec{\epsilon}_s$ (i.e., $\cos\theta=0$) and most slowly when $\delta\vec{\epsilon}=\pm\vec{\epsilon}_s$ (i.e., $\cos\theta=\pm1$); for $\delta\epsilon=\pm\hat{\epsilon}_s$, the decay is slightly faster when $\delta\vec{\epsilon}>0$ ($\cos\theta=\pm1$) and slightly slower when $\delta\vec{\epsilon}<0$ ($\cos\theta=-1$). The reason for this asymmetric peak is the fact that we have an isotropic Gaussian diffusion process in position space which is mapped into the electric field space by the anisotropic mapping specified in Eq. (2.13).

Thus the single-ion model and the weak diffusion model are similar (for small t and large $\vec{\epsilon}$ and $\vec{\epsilon}_0$) in that the conditional probability is represented by a function which is peaked about some point in the ϵ_0 direction and this peak broadens and shifts toward $\vec{\epsilon}=0$ as time increases. The peak is isotropic about its maximum value for the weak diffusion model defined by Eq. (2.8) because this model represents isotropic diffusion in electric field space. The peak is anisotropic for the single-ion model, Eq. (2.17), because it is based on isotropic diffusion in position space which is anisotropically mapped into the electric field space. Finally, neither of these models resembles in any way the strong diffusion process discussed in Sec. II A.

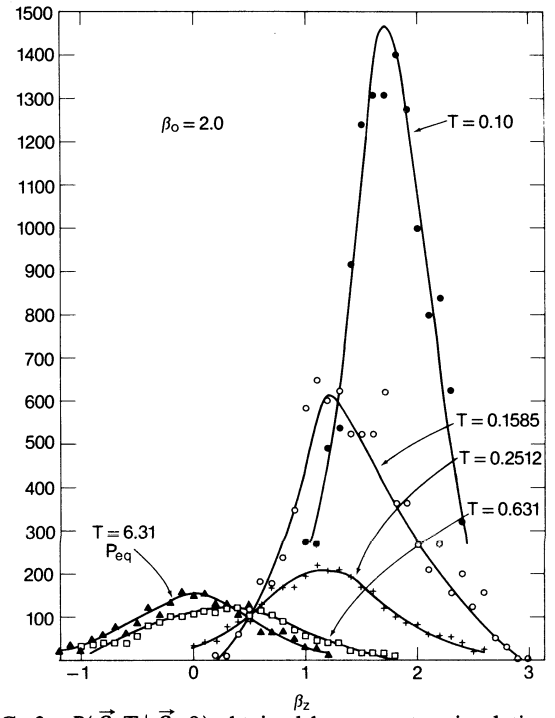

FIG. 3. $P(\vec{\beta},T\mid\vec{\beta}_0,0)$ obtained by computer simulation for an initial field strength $\beta_0=2$. Cylindrical coordinates are used for $\vec{\beta}$ with the β_z axis defined by the direction of the initial field; $\beta_\rho=0$ for all curves and P is independent of β_ϕ (i.e., cylindrically symmetric). Each curve is labeled by the normalized time variable $T=\omega_p t$ which ranges from $T=0.1$ to $T=6.31$ where $P=P_{eq}$. The solid curves are least-squares fits to the data.

III. COMPUTER SIMULATION

A. General considerations

The basic computer simulation technique discussed in Ref. 4 was employed in order to evaluate the conditional probability $P(\vec{\epsilon},t\mid\vec{\epsilon}_0,0)$ for some specific value of $\vec{\epsilon}_0$.

All computer simulation data presented in this paper were evaluated at a temperature of 10^4 K and an ion density $n=10^{17}$ cm^{-3} using 125 ions in a sphere of radius $5r_0$ where $4\pi r_0^3/3=n$. We have employed a dimensionless time variable $T=\omega_p t$, where $\omega_p=\sqrt{4\pi ne^2/m}$ is the ion plasma frequency, and a relative field vector

$$\vec{\beta}=\vec{\epsilon}/(e/r_0^2) \tag{3.1}$$

which employs the "normal field strength" e/r_0^2. To evaluate $P(\vec{\beta},t \mid \vec{\beta}_0,0)$ for a specific value of β_0, 125 position vectors $\vec{x}_j$ are chosen at random and the ion field is evaluated at the center of the sphere (i.e., the "test point") using the shielded field given in Eq. (1.5). If this field strength does not equal the specified value for β_0 to within ± 0.5, this configuration is rejected. When a configuration is found which produces the desired initial field strength, 125 velocity vectors $\vec{v}_j$ are then chosen and position vectors $\vec{r}_j(t)=\vec{x}_j+\vec{v}_j t$ are evaluated for a specified set of times t. The electric field is then evaluated for each time again using Eq. (1.5). This process is repeated until we have enough configurations to give a satisfactory noise level for the analysis of $P(\vec{\beta},T \mid \vec{\beta}_0,0)$. All data presented in this paper were obtained with 10 000 configurations for each value of β_0. By using a typical main frame computer (i.e., a CDC 6600 or a CYBER 750) 10 000 configurations and 14 values of time t required about 2000 sec for β_0 up to 8. Larger initial field strengths require slightly more time because the probability of finding an appropriate initial configuration decreases.

We have evaluated much more data than can be practically presented in this paper. A considerable amount of time was spent trying to find a simple analytic fit to the numerical data in the hope that it could all be presented by simply specifying a few coefficients for the fit. Thus far it has not been possible to obtain a satisfactory fit. We have therefore chosen to present those data which best illuminate the physical nature of the conditional probability function.

In representing $P(\vec{\beta},T \mid \vec{\beta}_0,0)$, we first note that P must be cylindrically symmetric about $\vec{\beta}_z$, the component parallel to $\vec{\beta}_0$. We therefore employ cylindrical coordinates in which β_ρ is the component perpendicular to $\vec{\beta}_0$, and β_z, the component parallel to $\vec{\beta}_0$.

In Figs. 3 and 4 we have plotted the conditional probability as a function of β_z with $\beta_\rho=0$. Several plots were made for various values of time T ranging from early times when the distribution is still peaked near the initial field strength β_0 to late times where P approaches P_{eq}.

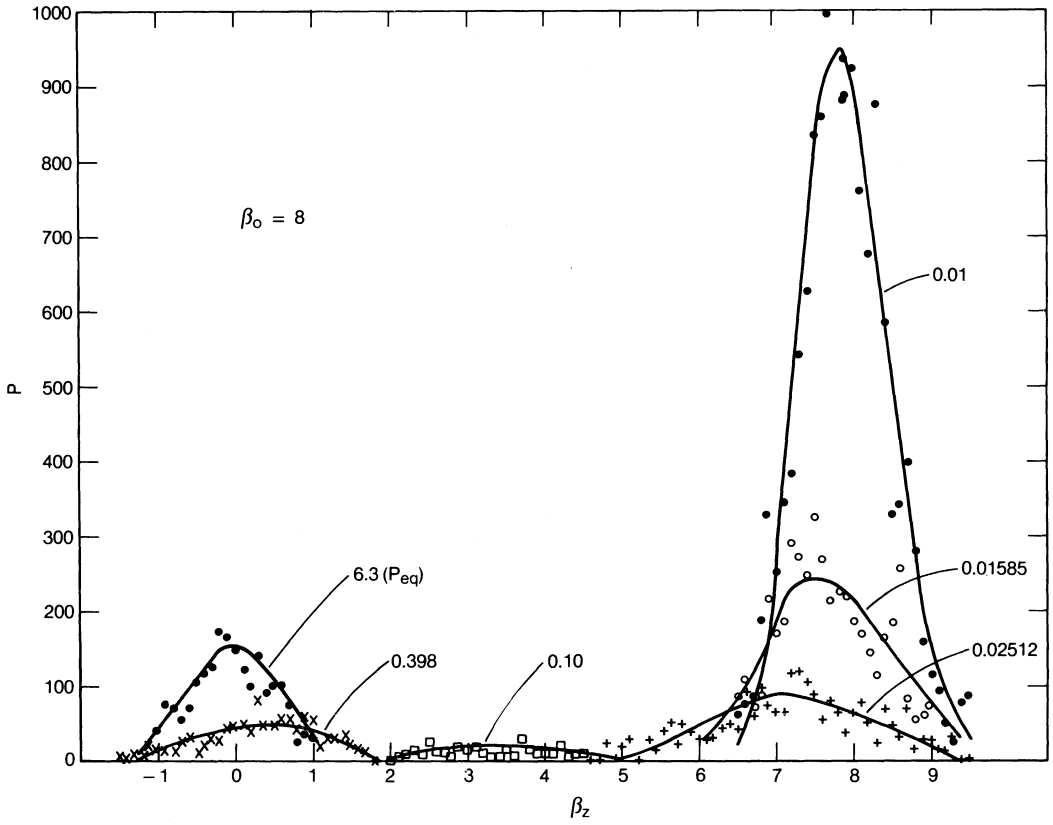

FIG. 4. $P(\vec{\beta},T \mid \vec{\beta}_0,0)$ obtained by computer simulation for an initial field strength $\beta_0=8$. Cylindrical coordinates are used for $\vec{\beta}$ with the β_z axis defined by the direction of the initial field; $\beta_\rho=0$ for all curves and P is independent of β_ϕ (i.e., cylindrically symmetric). Each curve is labeled by the normalized time variable $T=\omega_p t$ which ranges from $T=0.01$ to $T=6.3$ where $P=P_{eq}$. The solid curves are least-squares fits to the data.

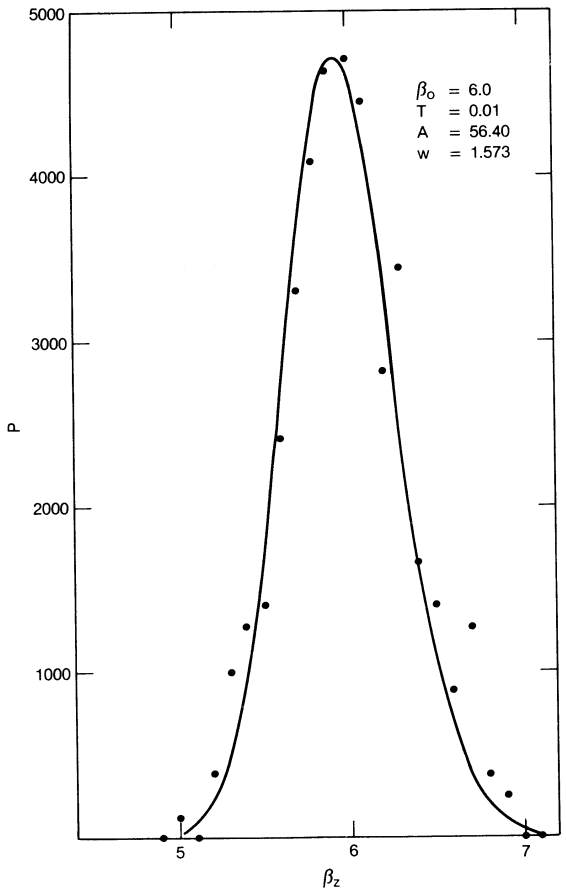

FIG. 5. P_1 fit to computer simulation data plotted as a function of β_z with $\beta_\rho=0$ and β_ϕ arbitrary.

Figure 3, which corresponds to an initial field strength $\beta_0=2$, looks rather similar to the weak diffusion behavior shown in Fig. 2 in that the peak broadens and shifts toward $\beta=0$ as T increases. In Fig. 3 however, the peak does not decrease monotonically with T but instead the peak height reaches a minimum for values of T near 0.4—0.6; the peak height then increases as P approaches P_{eq}. For the larger initial field strength, $\beta_0=8$, Fig. 4 shows a somewhat similar behavior but here the peak height at its minimum is much lower than in Fig. 3. The reason for this is that the peak is much broader for these intermediate times, that is, there are many more possible intermediate values of β when the initial field β_0 was large. For even larger values of β_0 the peak becomes broader and lower at the intermediate times and the situation begins to resemble the strong diffusion case illustrated in Fig. 1 except that the true peak near β_0 is not actually a delta function. It is also interesting to note that the initial peak near β_0 decays much more rapidly for the larger values of β_0. This is due to the fact that large initial fields tend to be produced by a single ion which is close to our test point whereas weak initial fields are dominated by a small group of ions which are not initially very close. For large β_0, the peak decays as the ion which dominates the initial field moves away from the test point at velocity v; for smaller x_0, a given value of vt produces a proportionally larger change in $\vec{r}(t)=\vec{x}_0+\vec{v}t$ hence the peak decays more rapidly for larger values of β_0. For small values of β_0, the ions in the group which initially dominates the electric field are slightly farther away hence one or more of these ions may move closer to our test point while others move away; the decay of the peak is thus considerably slower when the initial field is dominated by several ions.

From Figs. 3 and 4 it appears that there are two relatively independent physical processes which govern the time development of the conditional probability function. The first is the decay of the initial sharp peak near β_0 due to the ions which are near the test point at $T=0$. The second feature is the rise of the equilibrium peak at late times which is due to the inward diffusion of particles that were initially far away from the test point. Each of these processes will be examined separately.

B. Decay of the initial peak

In Figs. 5—12 we have used the modified single-particle function Φ_1 as given by Eq. (2.17) in order to fit the computer simulation data. We would expect the single-ion approximation to give a good fit for large values of β_0 which are known to be determined primarily by a single ion close to the test point. We also expect this fit to break down as time increases due to the increasing influence of other ions. In Figs. 5—11, $\beta_\rho=0$ and Eq. (2.17) reduces to

$$P_1(0,\beta_z,T;\beta_0)=(A/\beta_z^{9/2}w^3T^3)\times\exp[-(1/\sqrt{\beta_z}-1/\sqrt{\beta_0})^2/(wT)^2]\,, \quad (3.2)$$

where A and w are treated as adjustable parameters.

Figures 5 and 6 illustrate the general behavior of the P_1 fit. At early times and for a moderately large β_0, e.g., Fig. 5, the peak is very sharp, the maximum lies close to β_0 and the P_1 fit is quite good. As the peak broadens and

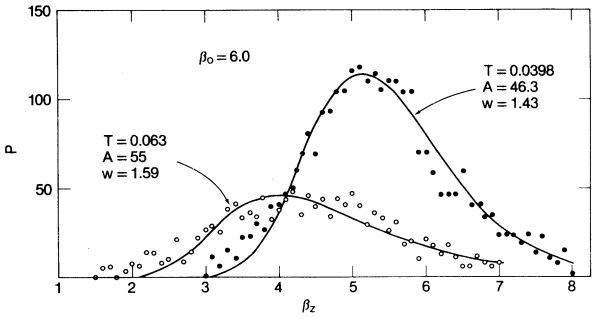

FIG. 6. P_1 fit to computer simulation data plotted as a function of β_z with $\beta_\rho=0$ and β_ϕ arbitrary.

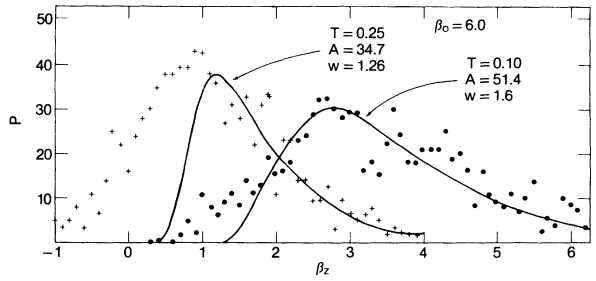

FIG. 7. P_1 fit to computer simulation data plotted as a function of β_z with $\beta_\rho = 0$ and β_ϕ arbitrary.

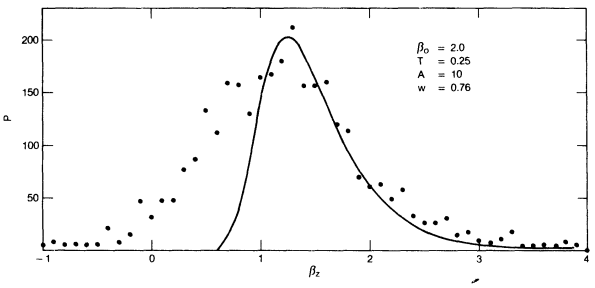

FIG. 9. P_1 fit to computer simulation data plotted as a function of β_z with $\beta_\rho = 0$ and β_ϕ arbitrary.

shifts, Figs. 6 and 7 show that the P_1 fit begins to break down for points on the small β_z side of the peak. For $T > 0.25$, the peak height has passed its minimum, the equilibrium peak is beginning to rise up out of the noise and the P_1 fit breaks down rapidly.

Figure 8 shows that the P_1 fit is quite good even for $\beta_0 = 2$ if T is small and the peak is very sharp. In Fig. 9 the peak is still fairly sharp but the fit is beginning to break down for small β even though the peak height has not yet reached its minimum (cf. Fig. 3.) Figures 10 and 11 were included in order to show that, for $\beta_0 \lesssim 1$, the P_1 fit is not very good even when the peak is extremely sharp.

We next consider the asymmetry in the initial peak. That is, even though $P(0,\beta_z,T;\beta_0)$ may be peaked about some value of β_z, say $\beta_s(\beta_0,T)$, P is not an isotropic function of $|\vec{\beta} - \beta_s\hat{\beta}_z|$ as the weak diffusion, Eq. (2.8), and strong diffusion, Eq. (2.7), models had assumed. In Fig. 12 we have plotted the simulation data as a function of β_ρ for $\beta_0 = 6.0$ and $T = 0.04$ holding β_z fixed at $\beta_z = 5.1$; from Fig. 6 we see that the peak occurs at this value of β_z. Figure 12 shows that the P_1 fit is fairly good except for a discrepancy in the region $\beta_\rho > 0.8$ where P is small; the same type of discrepancy is observed in Fig. 6 for $\beta_z < 4.0$ but there is no comparable error observed for large β_z, say $\beta_z > 7$, in Fig. 6. Thus we see that the initial peak is asymmetric, it falls off most rapidly in the direction perpendicular to the initial field, β_ρ, it falls off rapidly in the direction of small β_z and more slowly for β_z greater than the peak position. This is not a very strong asymmetry but it is definitely observable and it is described fairly well but not perfectly by the P_1 fit.

In Figs. 5–12, we have been using the modified conditional probability function given by Eq. (2.17). That is,

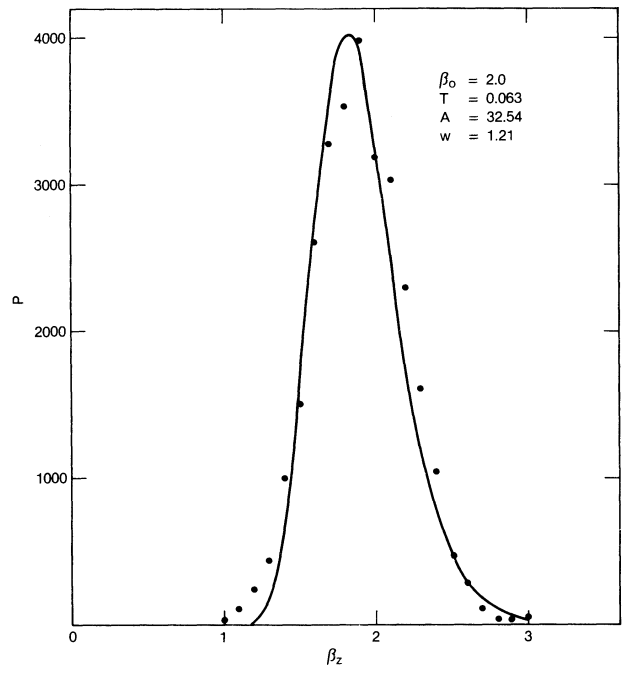

FIG. 8. P_1 fit to computer simulation data plotted as a function of β_z with $\beta_\rho = 0$ and β_ϕ arbitrary.

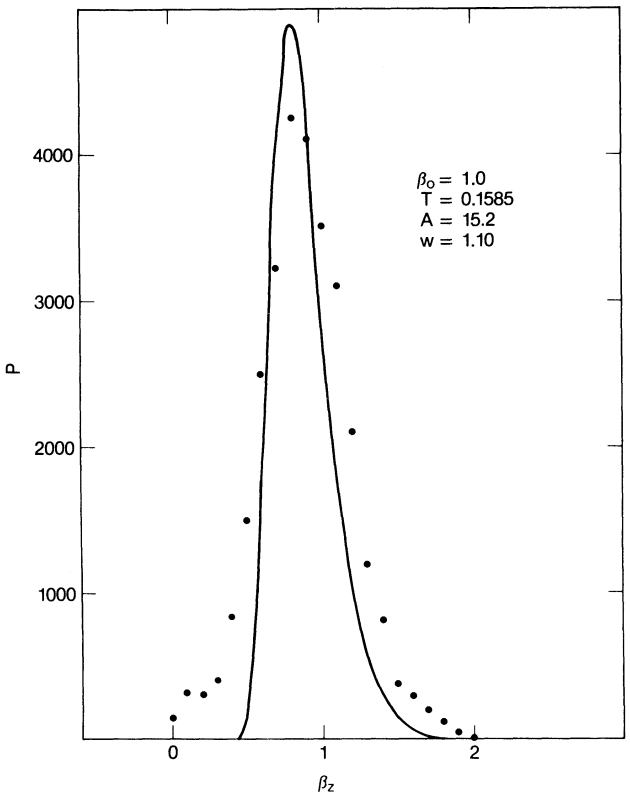

FIG. 10. P_1 fit to computer simulation data plotted as a function of β_z with $\beta_\rho = 0$ and β_ϕ arbitrary.

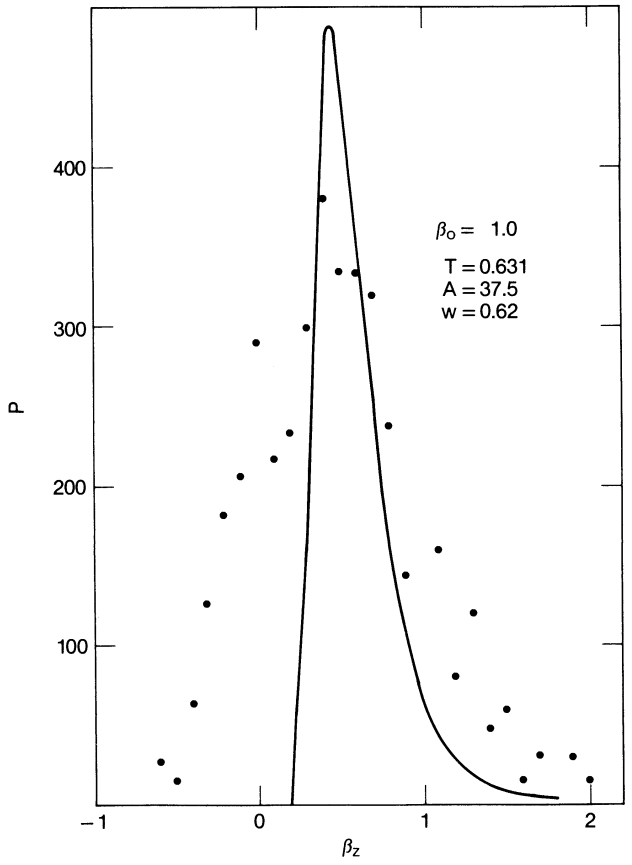

FIG. 11. P_1 fit to computer simulation data plotted as a function of β_z with $\beta_\rho=0$ and β_ϕ arbitrary.

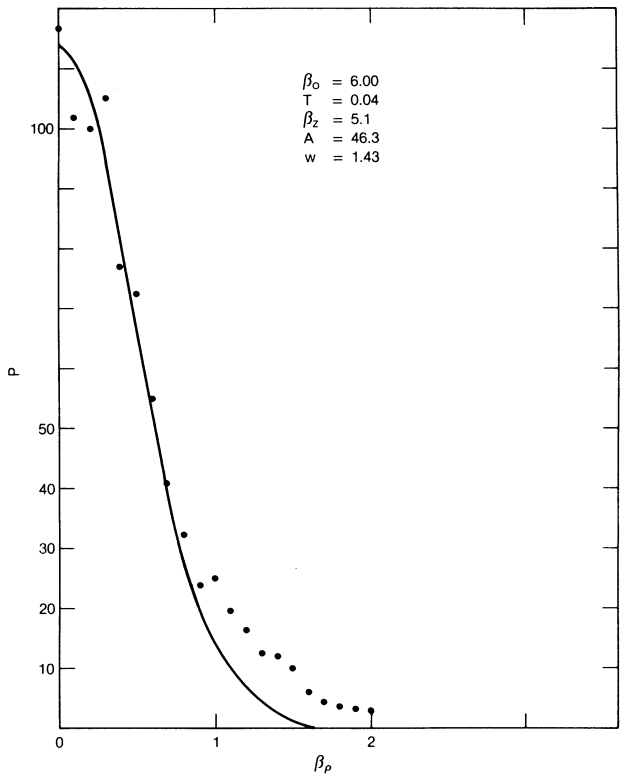

FIG. 12. P_1 fit to computer simulation data plotted as a function of β_ρ for $\beta_z=5.1$ and β_ϕ arbitrary.

the parameter w in Eq. (3.2) has been treated as an adjustable parameter to provide a fit to the computer simulation data. If the true single-particle Coulomb result, Eq. (2.15), had been used, w would have been fixed at the value $v_0/\sqrt{e}$ as noted in Sec. II C. This limit is indicated by the dashed line in Fig. 13 and it is seen that w does indeed approach the correct limit for small T and large β_0.

We may thus conclude that the initial peak is produced by those ions which are close to the test point at $T=0$. The decay and shift of this peak, as well as its asymmetry, may be fairly well represented by a function of the form

$$P_1(\vec{\beta},t \mid \vec{\beta}_0,0)=(A/\beta^{9/2}w^3T^3) \times \exp[-(\vec{\beta}/\beta^{3/2}-\vec{\beta}_0/\beta_0^{3/2})^2/(wT)^2] , \tag{3.3}$$

where w and A are treated as adjustable parameters. This function has the form of the result for a single ion producing a Coulomb field and, for large β_0 and small T where the single-ion approximation should be valid, w approaches the value 2.32 which corresponds to a single-ion approximation.

C. The rise of the equilibrium peak

We now turn to the "equilibrium" peak at $\vec{\beta}=0$ which rises up out of the noise for late times and approaches P_{eq} as $T\to\infty$. At the end of Sec. III A, we argued that this peak was dominated by the inward diffusion of ions that were initially far away from the test point. At first thought, it would seem that such a mechanism would produce a peak which is symmetric about $\vec{\beta}=0$. The computer simulation however produces a peak which is centered about some point $(\beta_\rho=0,\beta_z>0)$; for example, the peak for $T=0.398$ in Fig. 4 is rising out of the noise but it is clearly displaced in the direction of the initial peak at

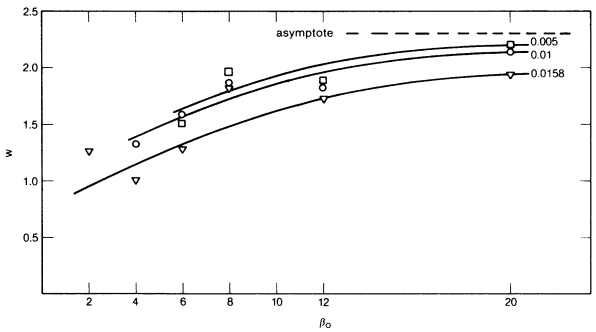

FIG 13. Width parameter w as a function of T and β_0. The asymptote indicated is the value obtained for a single-particle model using Coulomb fields.

$\vec{\beta}_0$. This would seem to imply some correlation between the "equilibrium" peak at large T and the initial peak at β_0. In order to understand this apparent correlation, we must look more closely at the joint probability distribution Φ defined in Eq. (1.6). A more detailed mathematical analysis of this function is given in the Appendix and we will only summarize the results of this analysis here.

In the Appendix, the function Φ is analyzed by separating the contributions from two groups of ions depending on their initial distance from the test point where the fields $\vec{\epsilon}$ are evaluated. Those ions initially within a distance λ_D are in the first group, while those initially more distant than λ_D are in the second group. The probability distribution which results from the distant ions is called $\Phi_>$ and the contribution from the close ions is called $\Phi_<$. The derivation leading to Eq. (A7) shows that Φ, and therefore also P, is given by the convolution of $\Phi_>$ and $\Phi_<$:

$$\Phi(\vec{\epsilon},t \mid \vec{\epsilon}_0,0)=\int d\vec{\epsilon}' \int d\vec{\epsilon}_0' \Phi_>(\vec{\epsilon}-\vec{\epsilon}',t \mid \vec{\epsilon}_0-\vec{\epsilon}_0',0) \times \Phi_<(\vec{\epsilon}',t \mid \vec{\epsilon}_0',0) . \quad (3.4)$$

A reasonable physical approximation to $\Phi_>$ is shown to be [see Eqs. (A15) and (A10)]:

$$\Phi_>(\vec{\epsilon},t \mid \vec{\epsilon}_0,0) \cong \delta(\vec{\epsilon}_0) f^{-2}(t) P_{\rm eq}(\epsilon / f^{2/3}(t)) , \quad (3.5)$$

where

$$f(t)=\int_{v<\lambda_D/t} d\vec{v}\, W(v) . \quad (3.6)$$

In the $t \to 0$ limit [see Eq. (A16)], this function goes to $\delta(\vec{\epsilon}_0)\delta(\epsilon)$ and Eq. (3.5) gives $\Phi \cong \Phi_<$.

Now we already know that Φ_1, as given by Eq. (2.17), is a good approximation to Φ for small t, hence it seems reasonable to approximate $\Phi_<$ by Φ_1 for all times t. Notice that we are not attempting to represent the complete distribution function Φ by Φ_1; this would be incorrect for large t as already noted. We are only replacing the contribution $\Phi_<$ by Φ_1.

We may thus analyze Φ for large times by using Eq. (3.4) with $\Phi_>$ given by Eq. (3.5) and $\Phi_<$ given by the modified Φ_1 of Eq. (2.17) or (2.18). In order to estimate the affect of the convolution in Eq. (3.4) we note that $P_{\rm eq}(\epsilon/f^{2/3}(t))$ is an approximately Gaussian function of width $f^{2/3}(t)$ peaked about $\vec{\epsilon}=0$ while Φ_1 is also an approximately Gaussian function [see Eq. (2.18)], peaked about $\vec{\epsilon}(t)$ having a width given by $wt\epsilon_s(t)/\sqrt{A}$ in Eq. (2.18). Since the convolution of two Gaussians is itself a Gaussian, we expect that Φ for late times will have a form given by

$$\Phi(\vec{\epsilon},t \mid \vec{\epsilon}_0,0)=\alpha^{-3}(t) P_{\rm eq}\{[\vec{\epsilon}-\vec{\epsilon}_s(t)/\alpha(t)]\} P_{\rm eq}(\epsilon) . \quad (3.7)$$

If we wish to relate the width of this function, α, to the widths of $\Phi_<$ and $\Phi_>$ we obtain

$$\alpha^2(t)=f^{4/3}(t)+w^2t^2\epsilon_s^2(t)/A . \quad (3.8)$$

As $t \to \infty$, $\epsilon_s(t) \to 0$, $wt\epsilon_s/\sqrt{A} \to 0$, and $f(t) \to 1$ and Eq. (3.7) approaches $P_{\rm eq}(\epsilon)P_{\rm eq}(\epsilon_0)$ which is the correct limit.

It is interesting to note that $wt\epsilon_s(t)/\sqrt{A}$ goes to zero in both the $t \to 0$ and $t \to \infty$ limits whereas $f(t)$ increases monotonically with t. This means that $\alpha(t)$ will always start from zero at $t=0$ and approach 1 as $t \to \infty$. For small values of ϵ_0 we find that α increases monotonically from 0 to 1 but for large ϵ_0, α increases to values greater than 1 for some range of t and then decreases to 1 as $t \to \infty$. In this sense, Eq. (3.7) is very similar to the weak

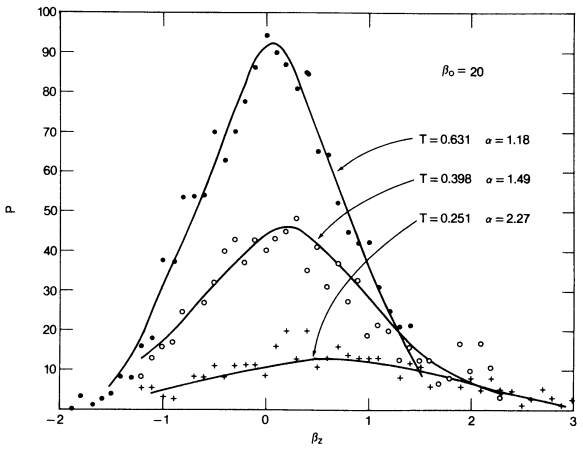

FIG. 14. Fit to computer simulation data for $\beta_0=20$ using Eq. (3.7). Results are plotted as a function of β_z for $\beta_\rho=0$ and β_ϕ arbitrary. Each curve is labeled by the normalized time variable T.

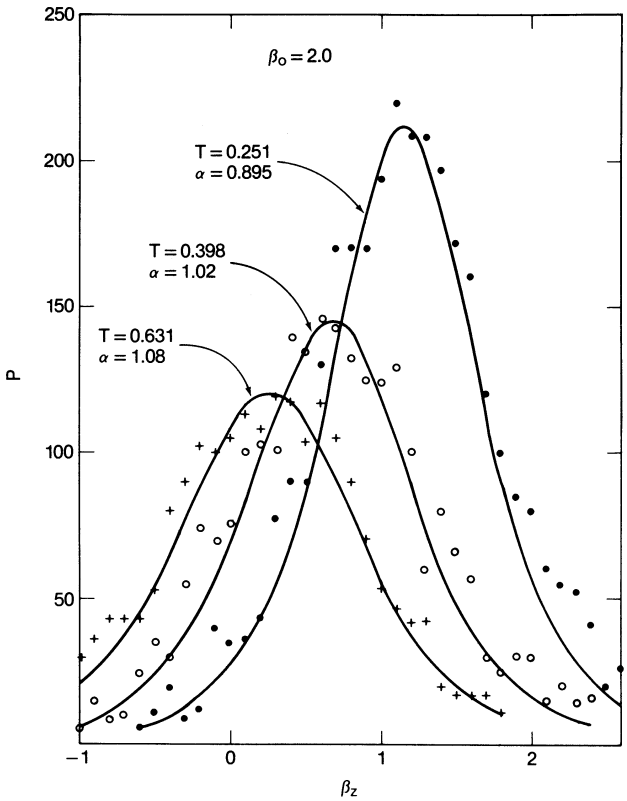

FIG. 15. Fit to computer simulation data for $\beta_0=2$ using Eq. (3.7). Results are plotted as a function of β_z for $\beta_\rho=0$ and β_ϕ arbitrary. Each curve is labeled by the normalized time variable T.

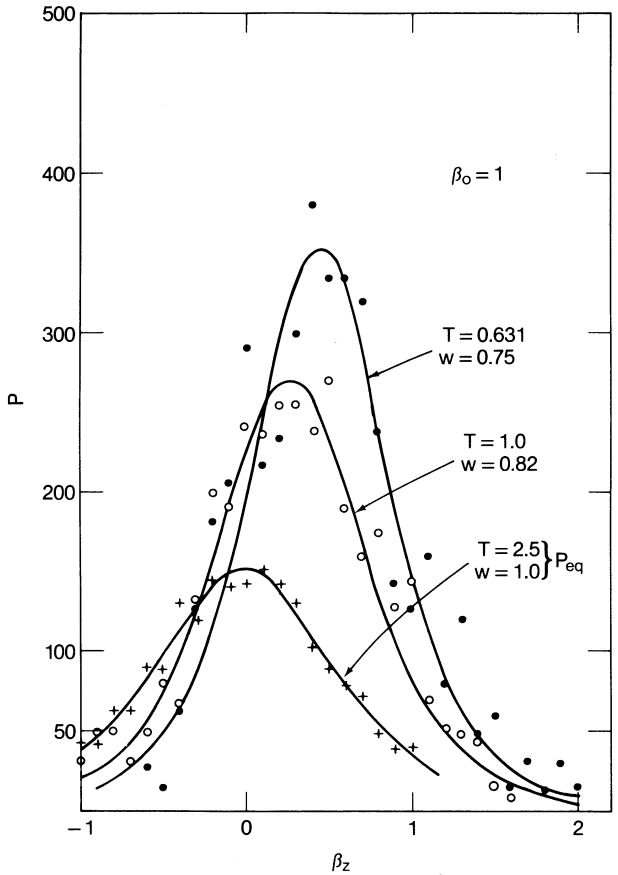

FIG. 16. Fit to computer simulation data for $\beta_0=1$ using Eq. (3.7). Results are plotted as a function of β_z for $\beta_\rho=0$ and β_ϕ arbitrary. Each curve is labeled by the normalized time variable T.

diffusion model discussed in Sec. II B except that the width was constrained to be a monotonically increasing function of time in that model, whereas $\alpha(t)$ is not always monotonic.

In Fig. 14 we show the fits obtained with Eq. (3.7) for a large initial field, $\beta_0=20$. In this case the equilibrium peak rises out of the noise near $\beta=0$ with very little shift or asymmetry observed. Similar results are seen in Fig. 4 for $\beta_0=8$ but there is a noticeable shift of the peak as it rises out of the noise. In Fig. 15, we have plotted the results for a relatively small value of β_0. In this case, the initial peak broadens and shifts with time and, for the range of data shown, α increases with time from 0.895 to 1.08; for $T>0.631$, α decreases to its asymptotic value of 1. This illustrates the property mentioned above, namely that $\alpha(t)$ does not always decrease monotonically with time as was assumed in the weak diffusion model. It is interesting to compare the $T=0.251$ result in Fig. 15 with the P_1 fit to the same data shown in Fig. 9; this comparison shows clearly that Eq. (3.7) provides a considerable improvement over the simple P_1 fit for late times. Figure 16 was included to show that, for small enough β_0, the width parameter $\alpha(t)$ does monotonically approach its asymptote, $\alpha=1$. Finally, Figs. 17 and 18 were included to show how a fit based on Eq. (3.7) will break down if we use it for small values of T. The main problem with such

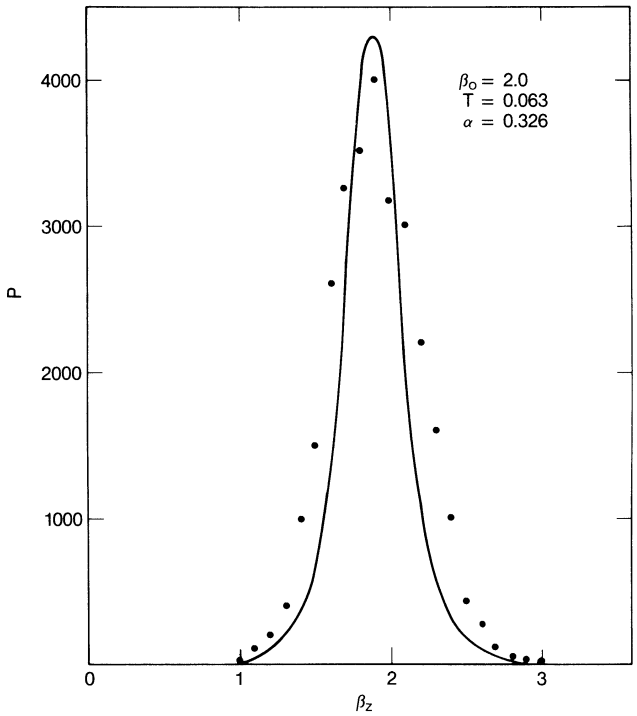

FIG. 17. Fit to computer simulation data using Eq. (3.7) plotted as a function of β_z for $\beta_\rho=0$ and β_ϕ arbitrary.

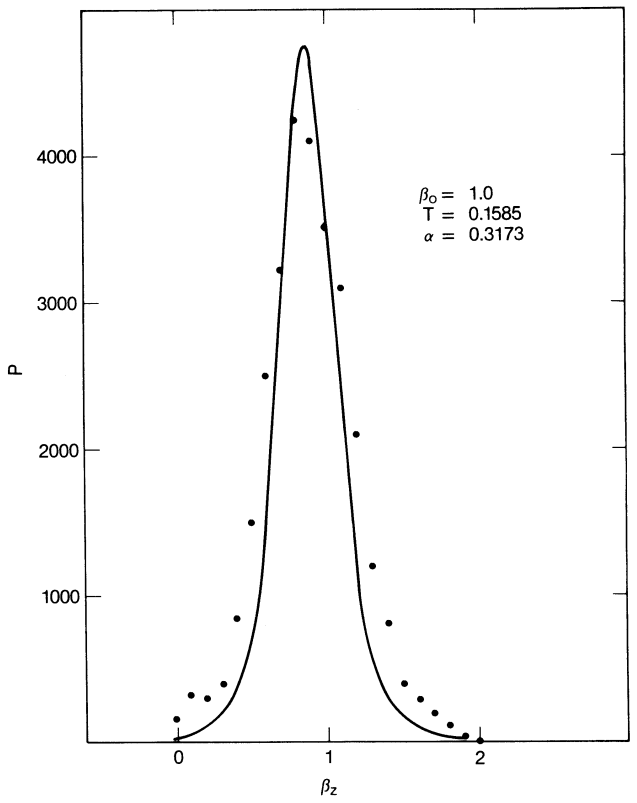

FIG. 18. Fit to computer simulation data using Eq. (3.7) plotted as a function of β_z for $\beta_\rho=0$ and β_ϕ arbitrary.

a fit is the lack of asymmetry in Eq. (3.7); this causes the theoretical function to fall off too slowly in the β_ρ direction (not shown) while it falls too rapidly in the β_z direction thus producing a profile which is too narrow in β_z and too wide in β_ρ. This problem, while observable, is never really serious and if one is not interested in the minor asymmetry effects, it is possible to obtain a reasonable fit to all of the data using Eq. (3.7).

The above argument shows that Φ and P are given by a convolution of functions $\Phi_>$ and $\Phi_<$ representing the effect of initially close and initially distant ions, respectively. For early times, the effect of the contribution from initially distant ions was well separated from the effect of the initially close ions because the functions $\Phi_>$ and $\Phi_<$ were sharply peaked about $\vec{\epsilon}=0$ and $\vec{\epsilon}_s$, respectively, and these two peaks did not interfere with one another. At late times, the peaks are broader and $\vec{\epsilon}_s(t)$ is approaching 0 hence the convolution does mingle these two functions to produce a result of the form given by Eq. (3.7).

IV. SUMMARY

In this paper we have used computer simulation and analytic techniques to examine the conditional probability function $P(\vec{\epsilon},t \mid \vec{\epsilon}_0,0)$ for the ion component of the plasma electric microfield.

At early times, $t \lesssim 1/\omega_p$, the function P is sharply peaked about some field $\vec{\epsilon}_s(t)=\epsilon_s(t)\hat{\epsilon}_0$. As t increases from 0 to $t \cong 1/\omega_p$, the peak height decreases, the width of the peak increases, and the location of the peak $\vec{\epsilon}_s$ decreases monotonically from $\vec{\epsilon}_s(t)=\vec{\epsilon}_0$ toward $\vec{\epsilon}_s(\infty)=0$.

As $t \to \infty$, $P(\vec{\epsilon},t \mid \vec{\epsilon}_0,0) \to P_{\rm eq}(\epsilon)$, where $P_{\rm eq}$ is the electric microfield distribution in three dimensions. If, during the course of its broadening and shifting, the initial peak height has fallen below its $t=\infty$ asymptotic value, i.e., $P_{\rm eq}(0)$, then at late times, $t > 1/\omega_p$, the peak height will start to increase and the width will decrease as t increases. For small initial field strengths, the peak height decreases monotonically to $P_{\rm eq}(0)$; it is only for larger values of ϵ_0 that one observes this initial decay of peak height followed a monotonic increase to $P_{\rm eq}(0)$.

An additional feature of this peak is that it is always slightly asymmetric, falling off most rapidly in the direction perpendicular to $\vec{\epsilon}_s$, less rapidly for $\epsilon < \epsilon_s$ when $\hat{\epsilon}=\hat{\epsilon}_0$, and least rapidly for $\epsilon > \epsilon_s$ when $\hat{\epsilon}=\hat{\epsilon}_0$. This asymmetry is explained by the fact than an isotropic diffusion of ions in position space does not produce an isotropic diffusion of electric fields.

We found that the strong diffusion model proposed by Brissaud and Frisch[10] does not give a good approximation to the actual conditional probability function. This observation lends support to the argument[3] that the MMM calculations[1,2] based on the Brissaud-Frisch model work well only when the details of the conditional probability function are not important, e.g., electron broadening, whereas the MMM begins to break down when the conditional probability becomes more important as in ion broadening. The strong diffusion model based on the renewal process proposed by Seidel[11] will probably give a poor approximation to the conditional probability function for the same reason.

We also found that the simple weak diffusion model proposed in Ref. 3 is not a good approximation for P either. The problem with this model is that the peak height must decrease monotonically with time and the peak is symmetric. The lack of asymmetry is not too serious but the monotonic decrease in peak height would be seriously wrong for moderate to large initial field strengths.

A simple analysis using a single-ion model with one adjustable parameter showed that the simulation data could be fit quite well by such a model for early times $t \lesssim 1/\omega_p$ and moderate to large initial field strengths (i.e., relative field strengths $\beta \geq 2$). This simple model even produces the asymmetry observed in the peak.

In order to get a better physical understanding of the observed data, an analytic analysis of the joint probability distribution function $\Phi(\vec{\epsilon},t \mid \vec{\epsilon}_0,0)$ was performed. The function Φ equals the conditional probability function P multiplied by $P_{\rm eq}(\epsilon_0)$, see Eq. (1.4). This analytic analysis showed that Φ, and therefore also P, is given by a convolution of functions $\Phi_<$ and $\Phi_>$ representing the effect of ions initially close to and initially distant from the test point where the electric field is evaluated [see Eq. (3.4)]. The diffusion of initially distant ions is statistically independent of the diffusion of the initially close ions; the effects of these two independent physical processes can be mingled by the convolution however. The function $\Phi_>$ is peaked about $\vec{\epsilon}=0$ [see Eq. (3.5)] whereas $\Phi_<$ is peaked about $\vec{\epsilon}_s(t)$ which shifts from $\vec{\epsilon}_0$ to 0 as t goes from 0 to ∞. At early times, the peaks in $\Phi_>$ and $\Phi_<$ are well separated and quite sharp so the convolution does not appreciably mingle the two physical processes. For early times, $\Phi_>$ is essentially just a delta function hence $\Phi \cong \Phi_< \cong \Phi_1$, where Φ_1 is the result for the single-ion model mentioned above; this result in fact suggests that $\Phi_<$ may be replaced by Φ_1 for all times. At late times, the two functions $\Phi_>$ and $\Phi_<$ (or Φ_1) have become broader and their peaks are now close together since $\epsilon_s(t) \to 0$ as $t \to \infty$. The convolution now succeeds in combining the effects of the initially distant ions with those of the initially close ions resulting in a function of the form [see Eq. (3.7)]

$$P(\vec{\epsilon},t \mid \vec{\epsilon}_0,0) \cong (1/\alpha^3) P_{\rm eq}\{[\vec{\epsilon}-\vec{\epsilon}_s(t)]/\alpha\} \quad t > 1/\omega_p \ . \tag{4.1}$$

Treating ϵ_s and α as adjustable parameters, this function provides a good fit to the simulation data although it lacks asymmetry which, for late times, becomes very small in any case.

The similarity between Eq. (4.1) and the weak diffusion model, Eq. (2.8), is striking; the primary difference between the two is in the fact that the width $\alpha(t)$ in Eq. (4.1) first increases with t for small t and then may decrease with t when t becomes large whereas the width would increase monotonically with t in the weak diffusion model.

These conclusions lead one to suspect that it will be possible to construct an analytic model which is a hybrid of Eq. (4.1) for late times and a weak diffusion model such as Eq. (2.8) or possibly $\Phi_1(\vec{\epsilon},t \mid \vec{\epsilon}_0,0)$ for early times. The application of such a model will hopefully be the subject of a future paper.

APPENDIX

It is possible to get a rough idea as to what the conditional probability function might look like by considering the theoretical expression given in Eq. (1.6). Using a Fourier representation for the delta functions in Eq. (1.6) and defining a function ϕ by

$$\phi(\vec{k},\vec{l},\vec{x}_j,\vec{r}_j)\equiv \exp[i\vec{k}\cdot\vec{\epsilon}_s(\vec{r}_j)+i\vec{l}\cdot\vec{\epsilon}_s(\vec{x}_j)]-1 , \tag{A1}$$

$$\Phi(\vec{\epsilon},t\mid\vec{\epsilon},0)=(2\pi)^{-6}\int d\vec{k}\int d\vec{l}\, e^{-i\vec{k}\cdot\vec{\epsilon}}e^{-i\vec{l}\cdot\vec{\epsilon}_0}V^{-N}\prod_j\int d\vec{x}_j\int d\vec{v}_j W(v_j)[1+\phi(\vec{k},\vec{l},\vec{x}_j,\vec{r}_j)]$$

$$=(2\pi)^{-6}\int d\vec{k}\int d\vec{l}\, e^{-i\vec{k}\cdot\vec{\epsilon}}e^{-i\vec{l}\cdot\vec{\epsilon}_0}V^{-N}[V+\phi(\vec{k},\vec{l})]^N , \tag{A2}$$

where $\phi(\vec{k},\vec{l})$ denotes the single-ion average

$$\phi(\vec{k},\vec{l})\equiv\int d\vec{x}\int d\vec{v}\, W(v)\phi(\vec{k},\vec{l},\vec{x},\vec{r})$$

$$=\int d\vec{x}\int d\vec{v}\, W(v)\{\exp[i\vec{k}\cdot\vec{\epsilon}_s(\vec{r})+i\vec{l}\cdot\vec{\epsilon}_s(x)]-1\} \tag{A3}$$

and we obtained a quantity raised to the Nth power in Eq. (A2) because all terms in the product over j are identical. Equation (A2) may be further developed by introducing the ion density $n=N/V$ and assuming that N is sufficiently large to permit

$$[1+n\phi(\vec{k},\vec{l})/N]^N\cong V^N\exp[n\phi(\vec{k},\vec{l})] . \tag{A4}$$

We thus obtain

$$\Phi(\vec{\epsilon},t\mid\vec{\epsilon}_0,0)=(2\pi)^{-6}\int d\vec{k}\int d\vec{l}\exp(-i\vec{k}\cdot\vec{\epsilon}-i\vec{l}\cdot\vec{\epsilon}_0)e^{n\phi(\vec{k},\vec{l})} . \tag{A5}$$

Equation (A5) is a very compact theoretical expression for the joint probability distribution and it is not beyond the realm of possibility to perform a numerical evaluation of this expression.

For our purposes, we will use Eq. (A5) as a starting point for various approximations which are designed to improve our physical insight concerning the conditional probability. We will start by simply writing ϕ in the form

$$\phi(\vec{k},\vec{l})=\phi_>(\vec{k},\vec{l})+\phi_<(\vec{k},\vec{l}) , \tag{A6}$$

where $\phi_>$ means $x>\lambda_D$ while $\phi_<$ means $x<\lambda_D$. Equation (A5) immediately becomes

$$\Phi(\vec{\epsilon},t\mid\vec{\epsilon}_0,0)=\int d\vec{\epsilon}'\int d\vec{\epsilon}'_0\Phi_>(\vec{\epsilon}_0-\vec{\epsilon}',t\mid\vec{\epsilon}_0-\vec{\epsilon}_0,t)\Phi_<(\vec{\epsilon}',t\mid\vec{\epsilon}'_0,0) , \tag{A7}$$

where

$$\Phi_<(\vec{\epsilon},t\mid\vec{\epsilon}_0,0)=(2\pi)^6\int\vec{d}k\int\vec{d}l\exp(-i\vec{k}\cdot\vec{\epsilon}-i\vec{l}\cdot\vec{\epsilon}_0)e^{n\phi_<(\vec{k},\vec{l})} \tag{A8}$$

and similarly $\Phi_>$ is the Fourier transform of $\exp(n\phi_>)$.

The function $\Phi_>$ is the probability distribution that would describe a situation in which all ions are initially outside a sphere whose radius is λ_D, the Debye length; the center of this sphere is of course the test point at which we are evaluating the electric fields $\vec{\epsilon}$ and $\vec{\epsilon}_0$. The function $\phi_>$ may be evaluated as follows:

$$\phi_>(\vec{k},\vec{l})=\int_{x>\lambda_D}d\vec{x}\int d\vec{v}\, W(v)\{\exp[i\vec{k}\cdot\vec{\epsilon}_s(r)+i\vec{l}\cdot\vec{\epsilon}_s(x)]-1\}$$

$$\cong\int_{x>\lambda_D}d\vec{x}\int d\vec{v}\, W(v)\{\exp[i\vec{k}\cdot\vec{\epsilon}_s(r)]-1\}$$

$$=t^{-3}\int_{x>\lambda_D}d\vec{x}\int dr\, W\left[\frac{\vec{x}-\vec{r}}{t}\right]\{\exp[i\vec{k}\cdot\vec{\epsilon}_s(r)]-1\}$$

$$=t^{-3}\int_{x>\lambda_D}d\vec{x}\left[\int_{\vec{r}<\lambda}d\vec{r}+\int_{\vec{r}>\lambda_D}d\vec{r}\right]W\left[\frac{\vec{x}-\vec{r}}{t}\right]\{\exp[i\vec{k}\cdot\vec{\epsilon}_s(r)]-1\}$$

$$\cong t^{-3}\int_{x>\lambda_D}d\vec{x}\, W\left[\frac{x}{t}\right]\int_{r<\lambda_D}d\vec{r}\{\exp[i\vec{k}\cdot\vec{\epsilon}_s(r)]-1\}$$

$$\cong f(t)\phi_{eq}(k) . \tag{A9}$$

In the first step we used $\vec{\epsilon}_s(x)\cong 0$ for $x>\lambda_D$, we then changed variables from $\vec{v}$ to $\vec{r}=\vec{x}+\vec{v}t$ and the $\vec{r}$ integral was divided into the regions $r<\lambda_D$ and $r>\lambda_D$; again using $\vec{\epsilon}_s(r)\cong 0$ for $\vec{r}>\lambda_D$ the latter contribution vanished. Finally, we replaced $\vec{x}-\vec{r}$ by x in W because $x>\lambda_D$. In the last line we simply defined two functions $f(t)$ and ϕ_{eq} by

$$f(t)=\frac{1}{t^3}\int_{x>\lambda_D} d\vec{x}\, W(x/t)=\int_{v>\lambda_D/t} d\vec{v}\, W(v)\ , \quad \text{(A10)}$$

$$\phi_{eq}(k)=\int_{r<\lambda_D} d\vec{r}\{\exp[i\vec{k}\cdot\vec{\epsilon}_s(r)]-1\}\ . \quad \text{(A11)}$$

The function ϕ_{eq} is essentially just the kernel for the equilibrium ion field distribution

$$P_{eq}(\epsilon)=(2\pi)^{-3}\int d\vec{k}\, e^{-i\vec{k}\cdot\vec{\epsilon}}\exp\{n\phi_{eq}(k)\}\ . \quad \text{(A12)}$$

This may be verified by comparing our Eqs. (A11) and (A12) with Eqs. (1), (6), (7), and (10) of Ref. 15, noting that the h_2 and higher-order terms in the Mozer-Baranger expansion provide a very small correction.

For a Coulomb field $\vec{\epsilon}_c(r)=e\vec{r}/r^3$, we could use $\vec{r}\,'=\vec{r}f^{1/3}$ to write

$$f(t)\int d\vec{r}\{\exp[i\vec{k}\cdot\vec{\epsilon}_c(r)]-1\}=\int d\vec{r}\{\exp[i\vec{k}\,'\cdot\vec{\epsilon}_c(r')]-1\}\ , \quad \text{(A13)}$$

where $\vec{k}\,'=\vec{k}f^{2/3}(t)$. Since $\vec{\epsilon}_c$ and $\vec{\epsilon}_s$ do not differ too radically for $r<\lambda_d$, we will use

$$n\phi_>(\vec{k},\vec{l})=n f(t)\phi_{eq}(\vec{k})\cong n\phi_{eq}(\vec{k}f^{2/3}(t)) \quad \text{(A14)}$$

so that, using Eq. (A12), Eq. (A8) reduces to

$$\Phi_>(\vec{\epsilon},t\,\vec{\epsilon}_0,0)\cong\delta(\vec{\epsilon}_0)\frac{P_{eq}(\epsilon/f^{2/3}(t))}{f^2(t)}\ . \quad \text{(A15)}$$

This is exactly the kind of contribution one might expect for those ions which are initially outside the Debye sphere; that is, since $f(t)\to 0$ as $t\to\infty$ and $f(t)\to 1$ as $t\to\infty$ [see Eq. (A10)] we must have

$$f^{-2}P_{eq}(\epsilon f^{2/3})\to\begin{cases}\delta(\epsilon) & \text{as } t\to 0\\ P_{eq}(\epsilon) & \text{as } t\to\infty\ .\end{cases} \quad \text{(A16)}$$

It is also useful to briefly investigate $\Phi_<$. In the limit of small t, we know that the single-ion model is a useful approximation; this approximation is obtained by using a series expansion in $n\phi$ and setting $N=1$

$$\begin{aligned}e^{n\phi_<}&\cong 1+n\phi_<+\cdots\\ &=1+n\int_{x<\lambda_D} d\vec{x}\int d\vec{v}\, W(v)\{\exp[i\vec{k}\cdot\vec{\epsilon}_s(r)+i\vec{l}\cdot\vec{\epsilon}_s(x)]-1\}\\ &\cong n\int d\vec{x}\int d\vec{v}\, W(v)\exp\{i\vec{k}\cdot\vec{\epsilon}_s(r)+i\vec{l}\cdot\vec{\epsilon}_s(x)\}\ .\end{aligned} \quad \text{(A17)}$$

To obtain the last line, we extended the $\vec{x}$ integral to infinity (since the integrand is essentially zero for $x>\lambda_D$) and used $n\int d\vec{x}=N=1$. Substituting this result into Eq. (A10) gives

$$\begin{aligned}\Phi_<(\vec{\epsilon},t\mid\vec{\epsilon}_0,0)&\to n\int d\vec{x}\int d\vec{v}\, W(v)\delta(\vec{\epsilon}-\vec{\epsilon}_s(r))\delta(\vec{\epsilon}-\vec{\epsilon}_s(x)) \quad \text{as } t\to 0\\ &=nP_1(\vec{\epsilon},t\mid\vec{\epsilon}_0 0)\ .\end{aligned} \quad \text{(A18)}$$

If we were to replace $\vec{\epsilon}_s$ by a Coulomb field this result would be identical to Eq. (2.13).

In the large-t limit, r becomes greater than λ_D and we may use $\epsilon_s(r)\cong 0$ to obtain

$$\begin{aligned}\Phi_<(k,l)&=\int_{x<\lambda_D} d\vec{x}\int d\vec{v}\, W(v)\{\exp[i\vec{k}\cdot\vec{\epsilon}_s(r)+i\vec{l}\cdot\vec{\epsilon}_s(x)]-1\}\\ &\cong\int_{x<\lambda_D} d\vec{x}\int d\vec{v}\, W(v)\{\exp[i\vec{l}\cdot\vec{\epsilon}_s(x)]-1\}\\ &=\phi_{eq}(l)\end{aligned} \quad \text{(A19)}$$

and

$$\Phi_<(\vec{\epsilon},t\,\vec{\epsilon}_0,0)\to\delta(\epsilon)P_{eq}(\epsilon_0) \quad \text{as } t\to\infty\ . \quad \text{(A20)}$$

Finally, combining Eq. (A7) with Eqs. (A16) and (A18) or with Eqs. (A15) and (A20) we obtain the limiting expressions for Φ:

$$\Phi(\vec{\epsilon},t\mid\vec{\epsilon}_0,0)\to nP_1(\vec{\epsilon},t\mid\vec{\epsilon}_0,0)P_{eq}(\epsilon_0) \quad \text{as } t\to 0 \quad \text{(A21)}$$

$$\Phi(\vec{\epsilon},t\mid\vec{\epsilon}_0,0)\to\frac{1}{f^2(t)}P_{eq}\left[\frac{\epsilon}{f^{2/3}(t)}\right]P_{eq}(\epsilon_0) \quad \text{as } t\to\infty\ . \quad \text{(A22)}$$

[1]J. Seidel, Z. Naturforsch **32a**, 1195 (1977).
[2]J. Seidel, Z. Naturforsch **32a**, 1207 (1977).
[3]E. W. Smith, B. Talin, and J. Cooper, J. Quant. Spectrosc. Radiat. Transfer **26**, 229 (1981).
[4]R. Stamm and E. W. Smith, Phys. Rev. A **30**, 450 (1984).
[5]C. F. Hooper, Jr., Phys. Rev. **165**, 215 (1968).
[6]G. H. Ecker and A. Schumacher, Z. Naturforsch. **30a**, 413 (1975).
[7]H. Capes and D. Voslamber, Phys. Rev. A **5**, 2528 (1972).
[8]W. R. Chappell, J. Cooper, and E. W. Smith, J. Quant. Spectrosc. Radiat. Transfer **10**, 1195 (1970).
[9]M. N. Rosenbluth and N. Rostocker, Phys. Fluids **5**, 776 (1962).
[10]A. Brissaud and U. Frisch, J. Quant. Spectrosc. Radiat. Transfer **11**, 1767 (1971).
[11]J. Seidel, Z. Naturforsch. **35a**, 679 (1980).
[12]D. R. Cox, *Renewal Theory* (Methuen, London, 1962). An equivalent discussion of renewal processes may be found in most advanced books on stochastic processes.
[13]J. Seidel, Ph.D. dissertation, Mathematisch-Naturwissenschaftlichen Fakultät der Universität Düsseldorf (1974).
[14]A. Brissaud, C. Goldbach, J. Leorat, A. Mazure, and G. Nollez, J. Phys. B **9**, 1129 (1976), especially Sec. 2.
[15]B. Mozer and M. Baranger, Phys. Rev. **118**, 626 (1960).